Scientia Iranica A (2021) 28(6), 3018–3029

Sharif University of Technology
Scientia Iranica
Transactions A: Civil Engineering
http://scientiairanica.sharif.edu

Development characteristics of corrugation at different passing speeds

Z.Q. Wang[a,b,*] and Z.Y. Lei[a,b]

a. *Institute of Rail Transit, Tongji University, Shanghai 201804, China.*
b. *Shanghai Key Laboratory of Rail Infrastructure Durability and System Safety, Tongji University, Shanghai 201804, China.*

Received 21 June 2020; received in revised form 14 March 2021; accepted 24 May 2021

KEYWORDS
Metro;
Corrugation;
Passing speed;
Vehicle-track coupled model;
Fixed frequency;
Wear development.

Abstract. By using the vehicle-track interaction model and the wear calculation model, the development characteristics of rail profile wear and the longitudinal characteristics of rail wear development of the track-vibration-absorber fastener tangential track at different passing speeds were analyzed. The results of rail profile wear analysis show that when the iteration times increases, the wear ranges and wear depths of left and right rails at the corrugation trough/crest position are close. Meantime, the wear depths of rail profile and wave depth amplitudes at the corrugation trough/crest position in discrete passing speed modes are significantly lower than those in constant passing speed mode. The results of rail longitudinal wear analysis show that with the increase of vehicle running times, the characteristic frequencies of corrugation do not change under different passing speed modes, which reflects the fixed frequency feature of corrugation, and the irregularity levels corresponding to characteristic frequencies of rail longitudinal wear under the three passing speed modes show a decreasing trend in turn. Compared with the constant passing speed mode, the discrete passing speed modes can significantly decrease the rail profile wear and the development degree of rail wear at the characteristic frequencies.

1. Introduction

Rail corrugation is a longitudinal periodic wave-like irregularity, which is one of the important causes for wheel-rail vibration and noise. It exists in the railway systems around the world and occurs in different degrees in the metro network [1–5]. Rail corrugation occurs in a wide range of sections, not only in the curve section but also in the tangent section and turnout section. Therefore, how to suppress and eliminate corrugation has become one of the urgent problems to be solved in the metro operation.

Scholars from all over the world have conducted a lot of research on its generation and development characteristics. In 1993, Grassie and Kalousek [6] summarized the research progress of corrugation and proposed that the mechanism of corrugation can be divided into fixed wavelength mechanism and material damage mechanism. At the same time, the mechanisms and treatment countermeasures of various types of corrugations were expounded. Later, Grassie modified the fixed wavelength mechanism into the fixed frequency mechanism [7,8]. Tanaka and Miwa [9] investigated an efficient periodic grinding management method for rail corrugation. In view of the serious inner rail corrugation of a South Africa freight line,

*. *Corresponding author. Tel.: +86 18621802301*
E-mail addresses: 1733359@tongji.edu.cn (Z.Q. Wang); leizhenyu@tongji.edu.cn (Z.Y. Lei)

doi: 10.24200/sci.2021.56238.4618

through complex eigenvalue analysis, Fourie et al. [10] found that in the case of large transverse creep, the coupling mode of the pitching mode of traction motor and the antisymmetric bending mode of wheelset was the reason for rail corrugation. Sadeghi et al. [11] studied the influence of rail irregularity wavelengths and amplitudes on the riding comfort by using the numerical model of vehicle-slab track interaction for parameter analysis, and the results illustrated that short-wavelength irregularities had a considerable influence on the riding comfort of slab tracks. Jin team had made a systematic study on rail surface defects, including rail scratch, rail surface random irregularity, rail transverse geometric defects, etc. [12–14]. Yan et al. [15] conducted a numerical analysis on the track structure supported by trapezoid sleepers of the Beijing metro using the genetic algorithm. Chen et al. [16,17] systematically investigated the causes of corrugation by using the theory of self-excited vibration and put forward corresponding corrugation control measures. Yao et al. [18] investigated the features and limitations of existing grinding methods and put forward a new simple grinding method to achieve more accurate and effective rapid grinding. Hei [19] selected typical corrugation sections to test and study the fracture of fastener elastic strips, formulated reasonable treatment measures, and proposed suggestions for rail corrugation management. Liu and Wang [20] put forward a cause theory of rail corrugation of friction-induced torsional vibration and explained that most of the corrugations occurred on the inner rail. By numerical analysis and field test, Song et al. [21] discussed the solution to the excessive dynamic effect of the vehicle-track system caused by rail corrugation. Ma et al. [22] revealed the mechanism of corrugation according to the corrugation growth rate. It was concluded that the third-order bending of rail, the resonance between wheels, and the second-order bending resonance of wheelset were the main factors leading to corrugation. Wang and Wu [23] founded the multi wheel-slab track system model and studied the impact of the reflection of rail vibration wave between wheels of high resilient fastener track on rail corrugation from two aspects: the frequency spectrum analysis of multi wheel-rail interaction and the time-varying evolution process of simulated corrugation.

As there are many types of rail corrugations, and the generation mechanisms of different forms of rail corrugation are also different, how to effectively control the rail corrugation is particularly important. Therefore, this paper analyzes the development characteristics of rail profile wear and the longitudinal characteristics of rail wear under different passing speeds by establishing the vehicle-track coupled model and the wear calculation model, to provide guidance for corrugation treatment from the perspective of changing the vehicle passing speed distribution.

2. Vehicle-track coupled model

2.1. Vehicle model

The reference sources for structural parameters of Metro Type-A vehicles could be found in the field literature [24]. The multi-body mechanical software UM (Universal Mechanism) is used to build the vehicle model, including a car body, two bogies, and four wheelsets. These components are all regarded as rigid bodies, and each rigid body (car body, bogie, or wheelset) has 6 degrees of freedom in different directions, which are longitudinal moving, transverse moving, floating, rolling, shaking, and pitching respectively. The whole three-dimensional vehicle system model has 42 degrees of freedom. The wheel tread employs LM tread. The body and bogie, and bogie and wheelset are connected by spring-damping elements.

2.2. Track model

The track model adopts a 60 kg/m track flexible track, and the fastener is simulated as bushing force elements. In the slab part, a three-dimensional model is established by the software ABAQUS and imported into the UM by the fixed-interface modal synthesis technique. The connection between slab and foundation is also simulated by force elements. The parameters of track structure refer to the literature [25].

2.3. Wheel-rail contact model

The Kik-Piotrowski model is used for calculation, which can be used in the non-Hertz contact case [26]. The schematic diagram of the dynamics model is shown in Figure 1.

2.4. Wear calculation model

Based on the friction work theory, the calculation model of rail material wear is established [24]. The wear depth $d(x)$ of rail surface is shown in Eq. (1):

$$d(x) = \frac{KP(x)\Delta t}{A\rho}, \tag{1}$$

where K is the wear ratio coefficient, taking 1×10^{-9} kg/Nm [27]; $P(x)$ is the friction power at the position x; Δt is the time step; A is the area of contact zone; ρ is the density of rail material, taking 7800 kg/m^3.

In the above-mentioned model, the four wheels are running on each rail at the same time, and the wear depth corresponding to each wheel is accumulated in the rail fixed position, therefore, the wear depth $\Delta D(x)$ under a single operation can be expressed in Eq. (2):

$$\Delta D(x) = \sum_{i=1}^{4} d_i(x)(i = 1, 2, 3, 4), \tag{2}$$

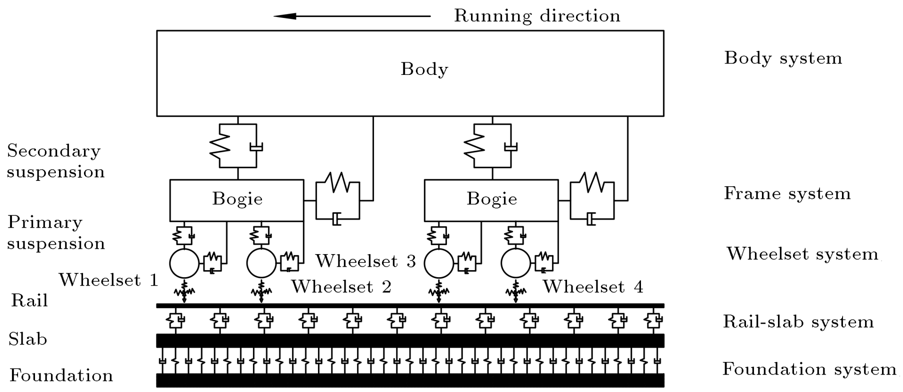

Figure 1. Schematic diagram of dynamics model.

where $d_i(x)$ $(i = i, 2, 3, 4)$ is the wear depth of each wheel in the rail fixed position. The wear depth $\Delta D(x)$ calculated by the single operation is added as the irregularity to the rail surface, therefore the next wear affected by the previous wear can be obtained. If the process is repeated, multiple rail surface superimposed wear can be obtained.

2.5. Model validation

Based on the above model, the simulation is conducted for a metro line, and the rail vertical vibration acceleration data at the measuring point is extracted and compared with the measured data, as shown in Figure 2. In the simulation process, the rail surface irregularity is measured using the measured rail surface irregularity, which is obtained by measuring the actual line with the corrugation acquisition instrument. The results show that simulation results are in good agreement with measurement results, which verifies the model validity.

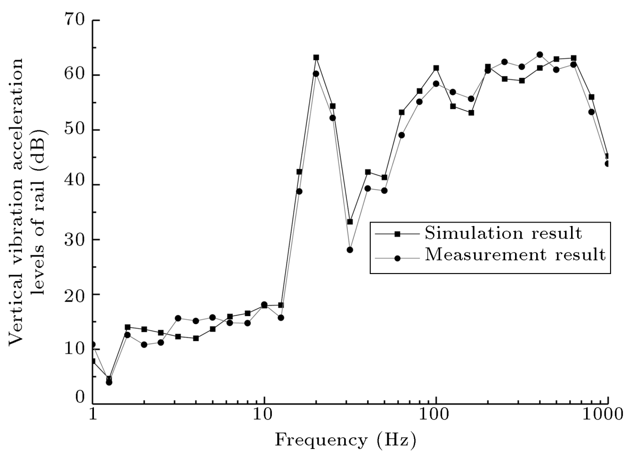

Figure 2. Results comparison diagram.

In view of this, the track-vibration-absorber fastener tangential track is selected as the research object, and the measured rail surface irregularity is applied on rails to study the development characteristics of rail profile wear and longitudinal characteristics of rail wear development under different passing speeds.

3. Passing speed modes

Through the establishment of three passing speed modes as shown in Table 1, the development characteristics of rail profile wear and the longitudinal characteristics of rail wear development are analyzed. By setting the weight value of the target passing speed, the distribution and development characteristics of rail wear under different passing speeds can be analyzed. The meaning of speed weight in Table 1 is the percentage of the number of wheels passing through the fixed rail profile under the target speed in the total number of wheels passing through or the percentage of the number of vehicles passing through the fixed line under the target speed in the total number of vehicles passing through. It should be noted that most of the vehicle running speeds on the metro tangential line are in the range of 40 km/h–80 km/h, therefore, in this paper, the distribution range of vehicle passing speeds, namely 40 km/h–80 km/h with an interval of 10 km/h is determined. Meantime, the setting of speed weights of three passing speed modes is mainly based on the principle that the weighted speed values of the three modes are equal.

Table 1. Passing speed modes.

Passing speed modes	Weights of speed (%)				
	40 km/h	50 km/h	60 km/h	70 km/h	80 km/h
Mode 1	0	0	100	0	0
Mode 2	30	0	40	0	30
Mode 3	20	20	20	20	20

4. Development characteristics of rail profile wear

4.1. Mode 1

Select the maximum rail wear depth of 0.1 mm as the basis for profile updating, and set the updating times as 10 times, and smooth the updated rail profile curve and cumulative wear curve, as shown in Figures 3 and 4. The trough position of rail corrugation is shown in Figures 3 and 4 ((a) and (b)) and the crest position of rail corrugation is shown in the same figures ((c) and (d)). The representations of Figures 5–8 are similar. It can be seen that, for both trough and crest positions, with the increase of the iteration times, the wear ranges of the left and right rails are similar, mainly within the range of −15 mm–15 mm in the transverse position of the rails. As for the trough position, the maximum wear depth of the left rail is 1.18 mm (2.82 mm in the transverse position of the rail), and the maximum increase of wear amount is 1.10 mm; the maximum wear depth of the right rail is 1.14 mm (2.82 mm in the transverse position of the rail), and the maximum increase of wear amount is 1.04 mm. As for the crest position, the maximum wear depth of the left rail is 0.86 mm (2.85 mm in the transverse position of the rail), and the maximum increase of wear amount is 0.84 mm; the maximum wear depth of the right rail is 0.85 mm (2.85 mm in the transverse position of the rail), and the maximum increase of wear amount is 0.76 mm. Furthermore, according to the above analysis, it can be concluded that the maximum wave depth amplitude of the left rail corrugation is about 0.32 mm, and the maximum wave depth amplitude of the right rail corrugation is about 0.29 mm.

4.2. Mode 2

The rail profile wear curve and cumulative wear curve after smoothing of passing speed Mode 2 are shown in Figures 5 and 6.

It can be seen from Figures 5 and 6 that, for both trough and crest positions, with the increase of the iteration times, the wear ranges of the left and right rails are basically within the range of −10 mm–15 mm in the transverse position of the rails. As

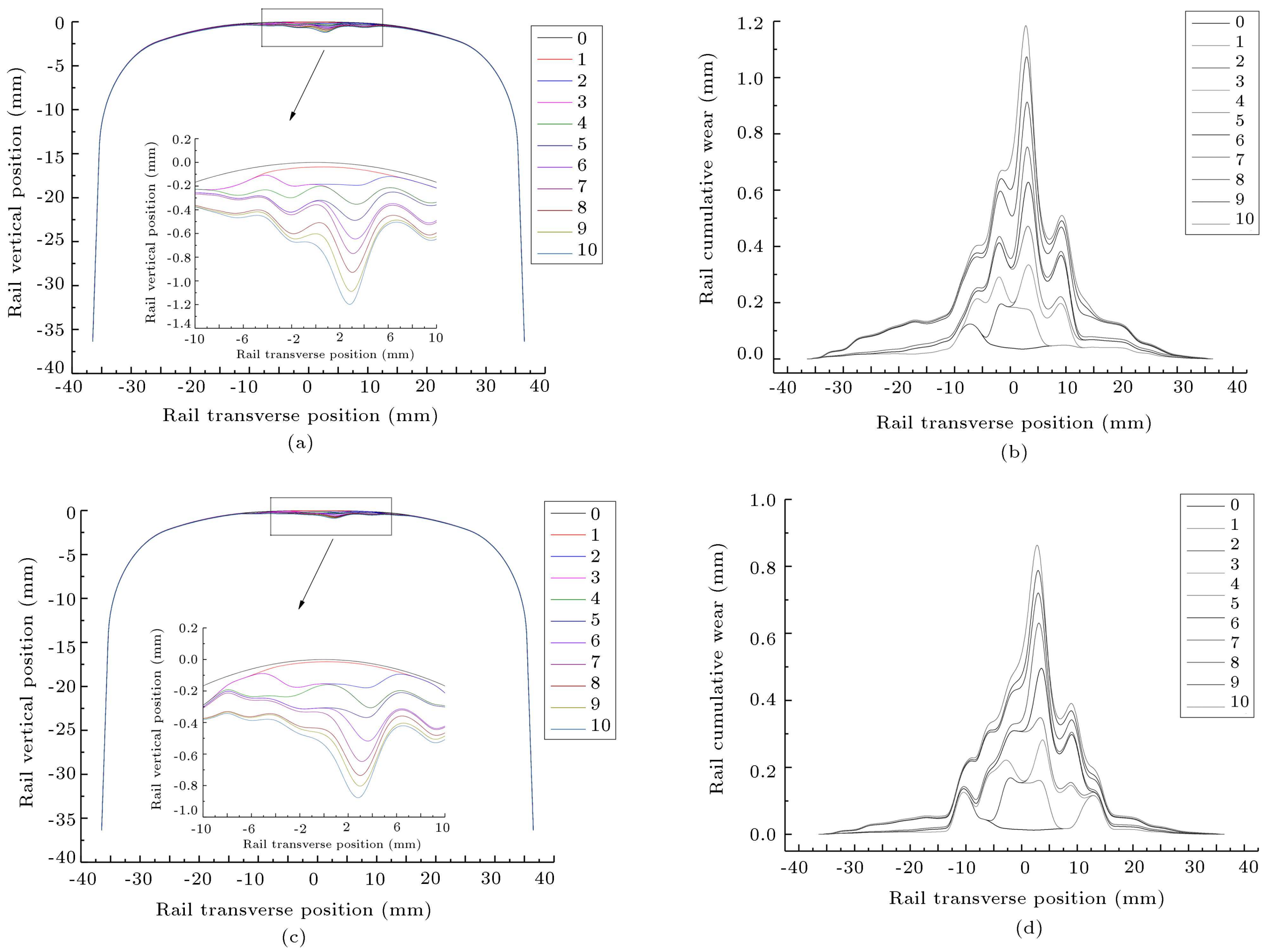

Figure 3. Left rail: (a) Rail profile diagram (trough), (b) rail cumulative wear diagram (trough), (c) rail profile diagram (crest), and (d) rail cumulative wear diagram (crest).

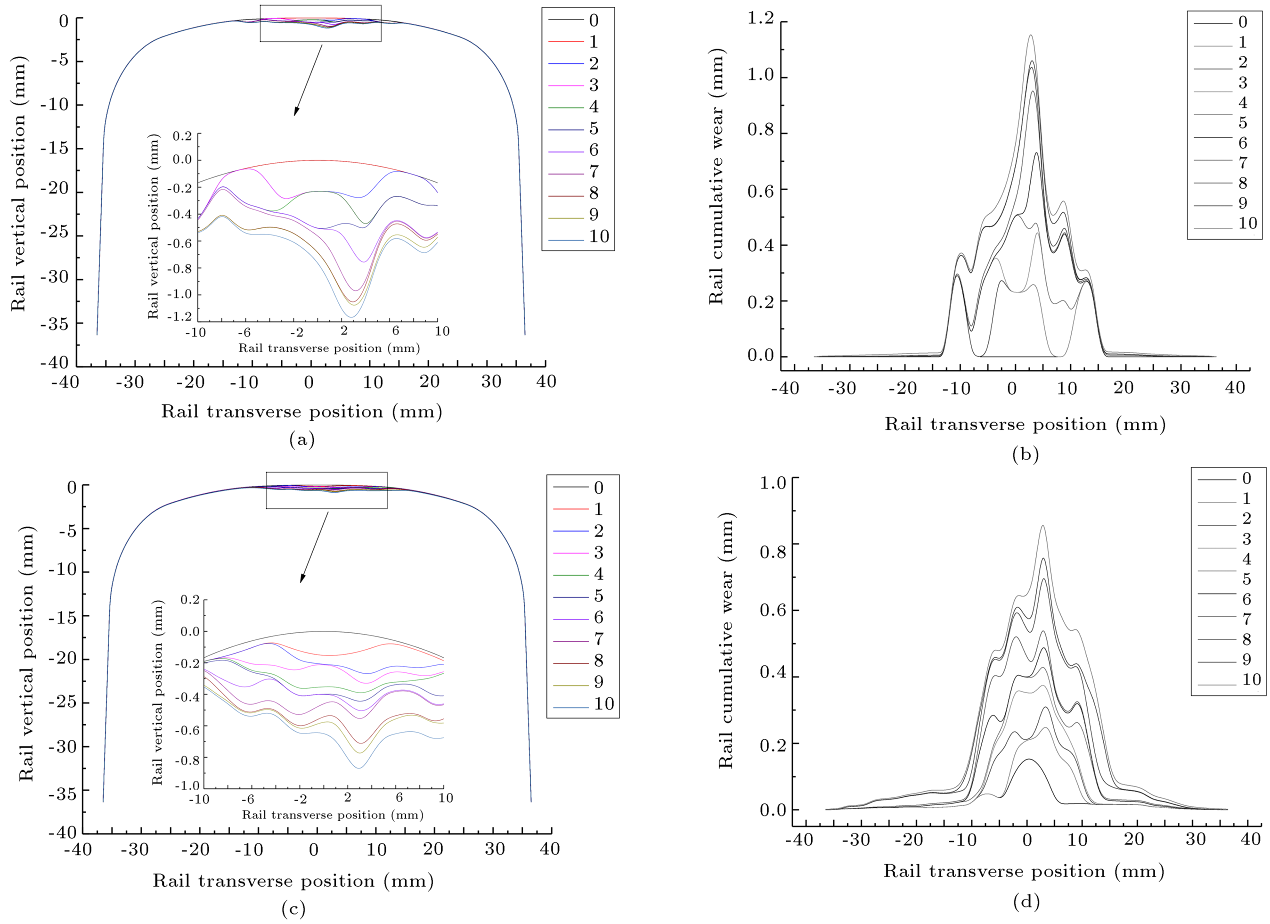

Figure 4. Right rail: (a) Rail profile diagram (trough), (b) rail cumulative wear diagram (trough), (c) rail profile diagram (crest), and (d) rail cumulative wear diagram (crest).

for the trough position, the maximum wear depth of the left rail is 0.31 mm (5.80 mm in the transverse position of the rail), and the maximum increase of wear amount is 0.20 mm; the maximum wear depth of the right rail is 0.30 mm (6.22 mm in the transverse position of the rail), and the maximum increase of wear amount is 0.19 mm. As for the crest position, the maximum wear depth of the left rail is 0.22 mm (5.86 mm in the transverse position of the rail), and the maximum increase of wear amount is 0.18 mm; the maximum wear depth of the right rail is 0.19 mm (3.01 mm in the transverse position of the rail), and the maximum increase of wear amount is 0.17 mm. Moreover, through the above analysis, it becomes clear that the maximum wave depth amplitude of the left rail corrugation is about 0.09 mm, and the maximum wave depth amplitude of the right rail corrugation is about 0.11 mm.

4.3. Mode 3

The rail profile wear curve and cumulative wear curve after smoothing of passing speed Mode 3 are shown in Figures 7 and 8.

It can be seen from Figures 7 and 8 that, for both trough and crest positions, with the increase of the iteration times, the wear ranges of the left and right rails are basically within the range of −12.5 mm–15 mm in the transverse position of the rails. As for the trough position, the maximum wear depth of the left rail is 0.31 mm (0.82 mm in the transverse position of the rail), and the maximum increase of wear amount is 0.20 mm; the maximum wear depth of the right rail is 0.29 mm (−0.53 mm in the transverse position of the rail), and the maximum increase of wear amount is 0.18 mm. As for the crest position, the maximum wear depth of the left rail is 0.22 mm (−0.01 mm in the transverse position of the rail), and the maximum increase of wear amount is 0.16 mm; the maximum wear depth of the right rail is 0.19 mm (−0.25 mm in the transverse position of the rail), and the maximum increase of wear amount is 0.15 mm. Moreover, based on the above analysis, it can be obtained that the maximum wave depth amplitude of the left rail corrugation is about 0.09 mm, and the maximum wave depth amplitude of the right rail corrugation is about 0.10 mm.

By comparing the distribution and development

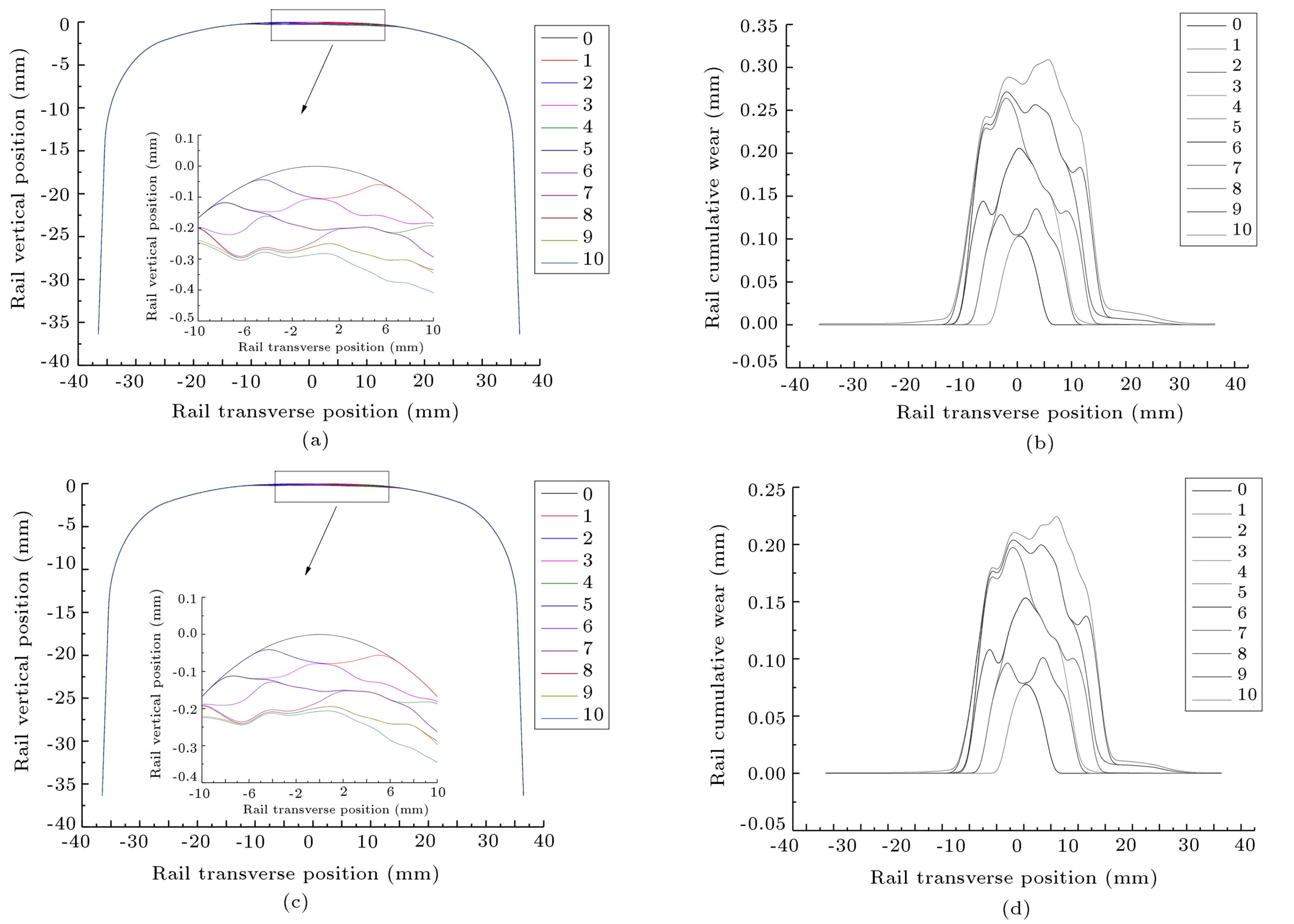

Figure 5. Left rail: (a) Rail profile diagram (trough), (b) rail cumulative wear diagram (trough), (c) rail profile diagram (crest), and (d) rail cumulative wear diagram (crest).

characteristics of rail wear under the above three passing speed modes, it is found that for the track-vibration-absorber fastener track, the rail profile wear depths and wave depth amplitudes at both trough and crest positions of rail corrugation of passing speed Modes 2 and 3 decreased significantly compared with those of Mode 1, which shows that the change of vehicle passing speed has a great influence on the rail profile wear of track-vibration-absorber fastener track. The discrete passing speed can significantly reduce the rail profile wear compared with the constant passing speed.

5. Longitudinal characteristics of rail wear development

This section mainly studies the longitudinal development characteristics of rail corrugation of the track-vibration-absorber fastener track under three passing speed distribution modes. According to the calculation results of rail profile wear, the wear distribution ranges and development trends of left and right rails are similar, therefore, in this section, the left side rail is considered to be the research object. Because the amount of wear caused by a single-running of single-vehicle is very small, the rail wear is recorded after 100,000, 300,000, and 500,000 single-vehicle running.

5.1. Mode 1

For the track-vibration-absorber fastener track, by using the wear calculation model for simulation, the rail wear development curve and its irregularity level spectrum (obtained by Fourier transform) of passing speed Mode 1 can be obtained, as shown in Figure 9.

The analysis shows that the characteristic frequencies of corrugation do not change with the increase of the vehicle operation times (the same for Sections 5.2 and 5.3). The main characteristic frequencies of corrugation corresponding to passing speed Mode 1 are 105 Hz (corresponding to the irregularity level of 37.67 dB) and 142 Hz (corresponding to the irregularity level of 36.89 dB), and the secondary characteristic frequencies are 70.7 Hz (corresponding to the irregularity level of 31.66 dB) and 35.7 Hz (corresponding to the irregularity level of 31.01 dB). The remaining partial peak frequencies and the corresponding irregularity levels are shown in Table 2, and most of these

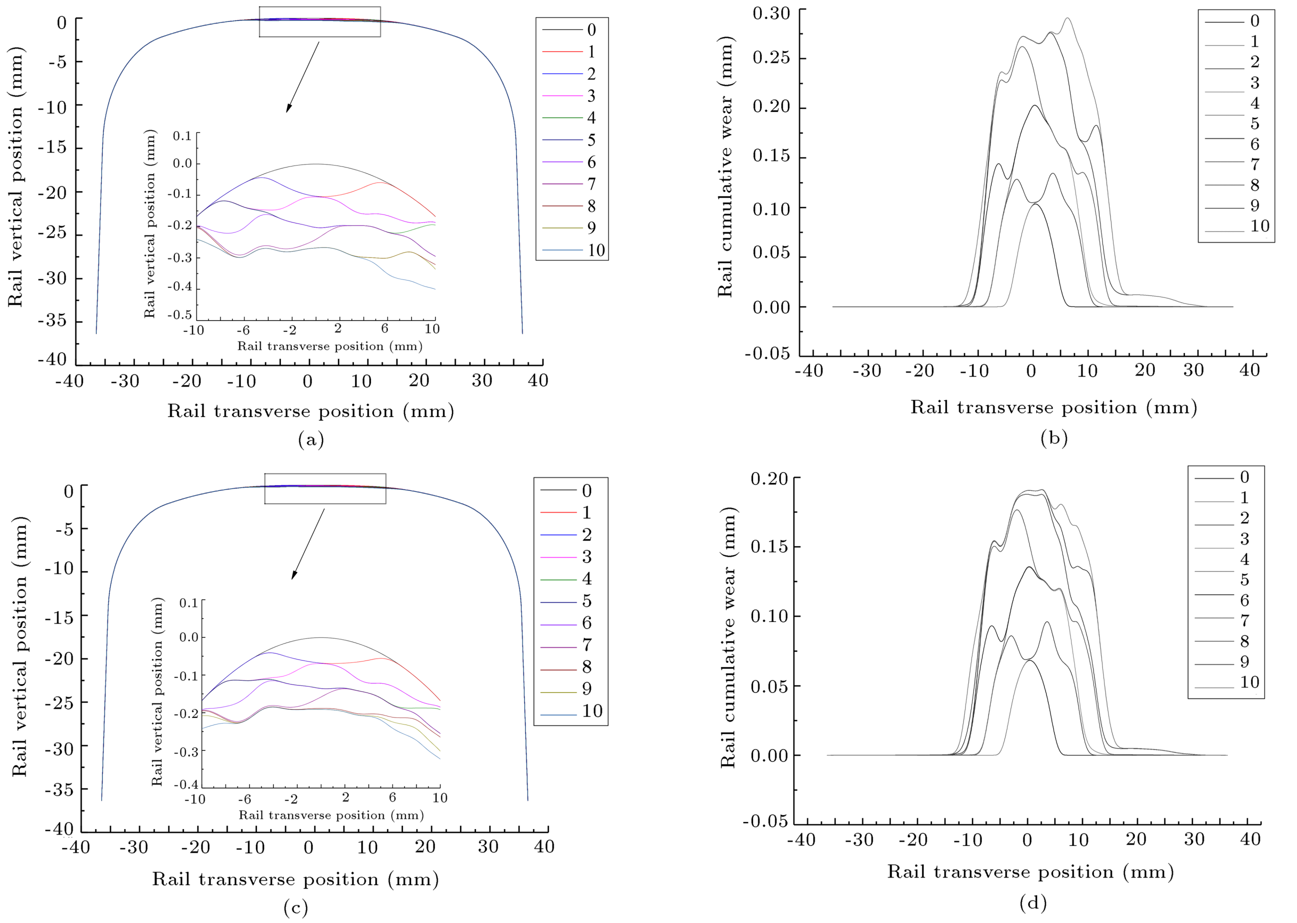

Figure 6. Right rail: (a) Rail profile diagram (trough), (b) rail cumulative wear diagram (trough), (c) rail profile diagram (crest), and (d) rail cumulative wear diagram (crest).

Table 2. Summary of remaining partial peak frequencies and corresponding irregularity levels.

Mode 1		**Mode 2**		**Mode 3**	
Peak frequencies (Hz)	**Irregularity levels (dB)**	**Peak frequencies (Hz)**	**Irregularity levels (dB)**	**Peak frequencies (Hz)**	**Irregularity levels (dB)**
212	25.61	107	29.12	178	17.03
248	24.22	177	22.81	239	17.73
283	24.07	213	24.07	286	15.76
383	21.82	249	22.40	321	19.28
460	16.76	284	22.80	387	14.35
531	17.60	384	20.56	482	11.97
632	16.61	475	15.07	582	11.82
708	16.34	556	14.24	626	12.40
		634	15.65	729	14.63
		711	16.34		

frequencies are related to the initial irregularity of the rail surface.

5.2. Mode 2

Similarly, by using the wear calculation model, the rail wear development curve and its irregularity level spectrum of passing speed Mode 2 are shown in Figure 10.

The main characteristic frequencies of corrugation corresponding to passing speed Mode 2 are 71.1 Hz (corresponding to the irregularity level of 37.47 dB) and 142 Hz (corresponding to the irregularity level of 36.77 dB), and the second characteristic frequency is 35.7 Hz (corresponding to the irregularity level of 33.35 dB). The remaining partial peak frequencies and the corresponding irregularity levels are also shown in Table 2.

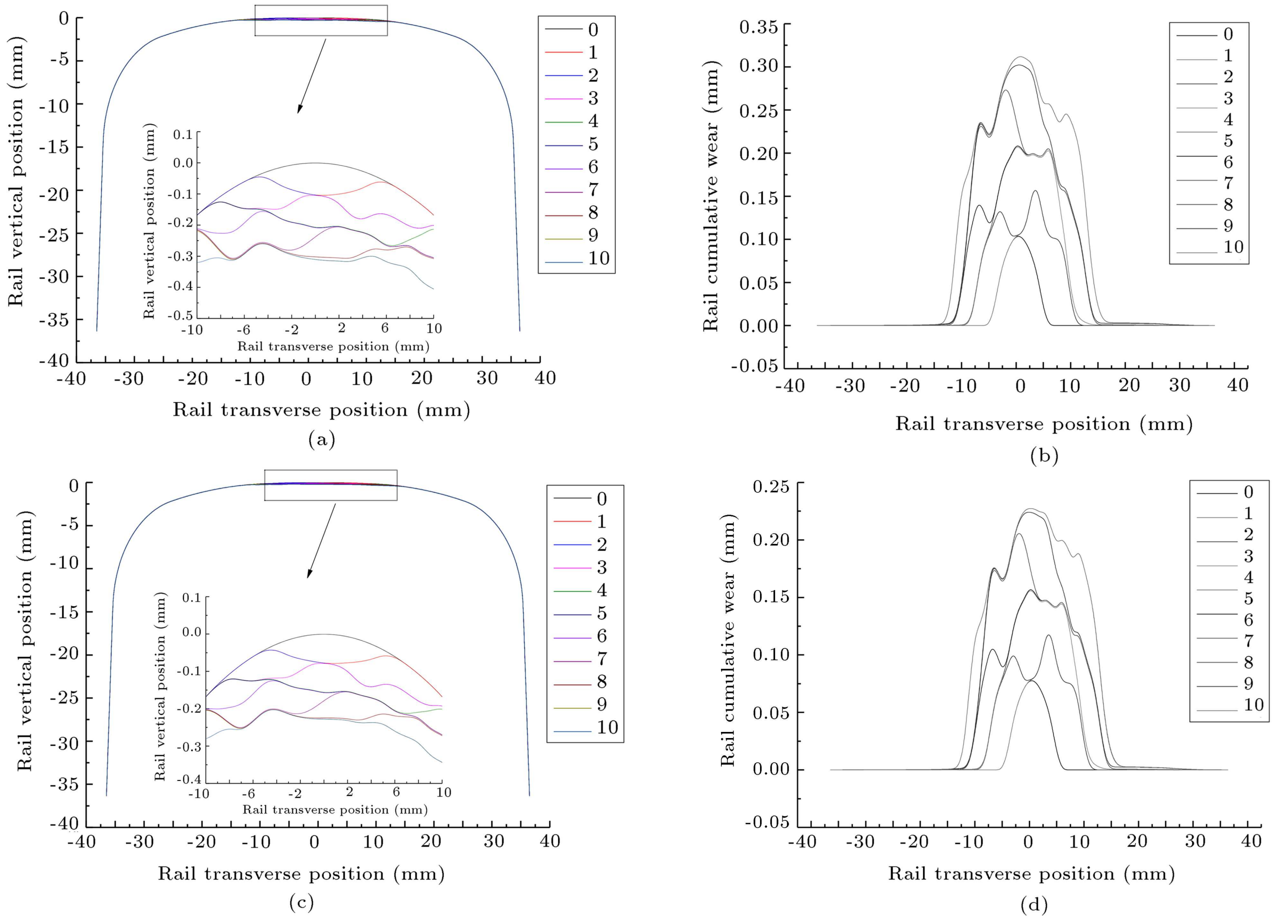

Figure 7. Left rail: (a) Rail profile diagram (trough), (b) rail cumulative wear diagram (trough), (c) rail profile diagram (crest), and (d) rail cumulative wear diagram (crest).

5.3. Mode 3

According to the wear calculation model, the rail wear development curve and its irregularity level spectrum of passing speed Mode 3 are shown in Figure 11.

The main characteristic frequencies of corrugation corresponding to passing speed Mode 3 are 143 Hz (corresponding to the irregularity level of 32.78 dB), 32.1 Hz (corresponding to the irregularity level of 31.23 dB), and 18.7 Hz (corresponding to the irregularity level of 31.08 dB), and the secondary characteristic frequencies are 71.5 Hz (corresponding to the irregularity level of 26.31 dB) and 107 Hz (corresponding to the irregularity level of 24.59 dB). See Table 2 for the remaining partial peak frequencies and the corresponding irregularity levels.

By comparing the above results, it is found that for the track-vibration-absorber fastener track, with the increase of vehicle running times, the characteristic frequencies of corrugation do not change under different passing speed modes, which indicates the fixed frequency characteristic of corrugation. The fixed frequency mechanism of corrugation is subject to the inherent properties of the vehicle-track system, which shows that the characteristic frequencies of corrugation are constant, that is, the variation of vehicle speeds will not affect the characteristic frequencies of corrugation [8,28]. When the vehicle-track system is stimulated, the modal coupling resonances of the vehicle-track system at certain frequencies could be excited, and the rail corrugations at corresponding frequencies may be induced. The irregularity levels corresponding to characteristic frequencies of the longitudinal development of rail wear under three passing speed modes decrease in turn, which shows that the discrete passing speed modes can effectively decrease the development degree of rail wear at the characteristic frequencies compared with the constant passing speed mode.

In addition, comparing Figure 9(a) and Figure 10(a), it can be seen that in the line interval range of 40 m–50 m (only 10 m interval is intercepted for display in order to show clearly), when the number of vehicle runs is 500000, the rail wear in Mode 2 is greater than that in Mode 1 in some positions. The reason is mainly related to the sensitive speed corresponding to the rail wear, that is, the speed of 40 km/h and 80 km/h in Mode 2 will promote the rapid development

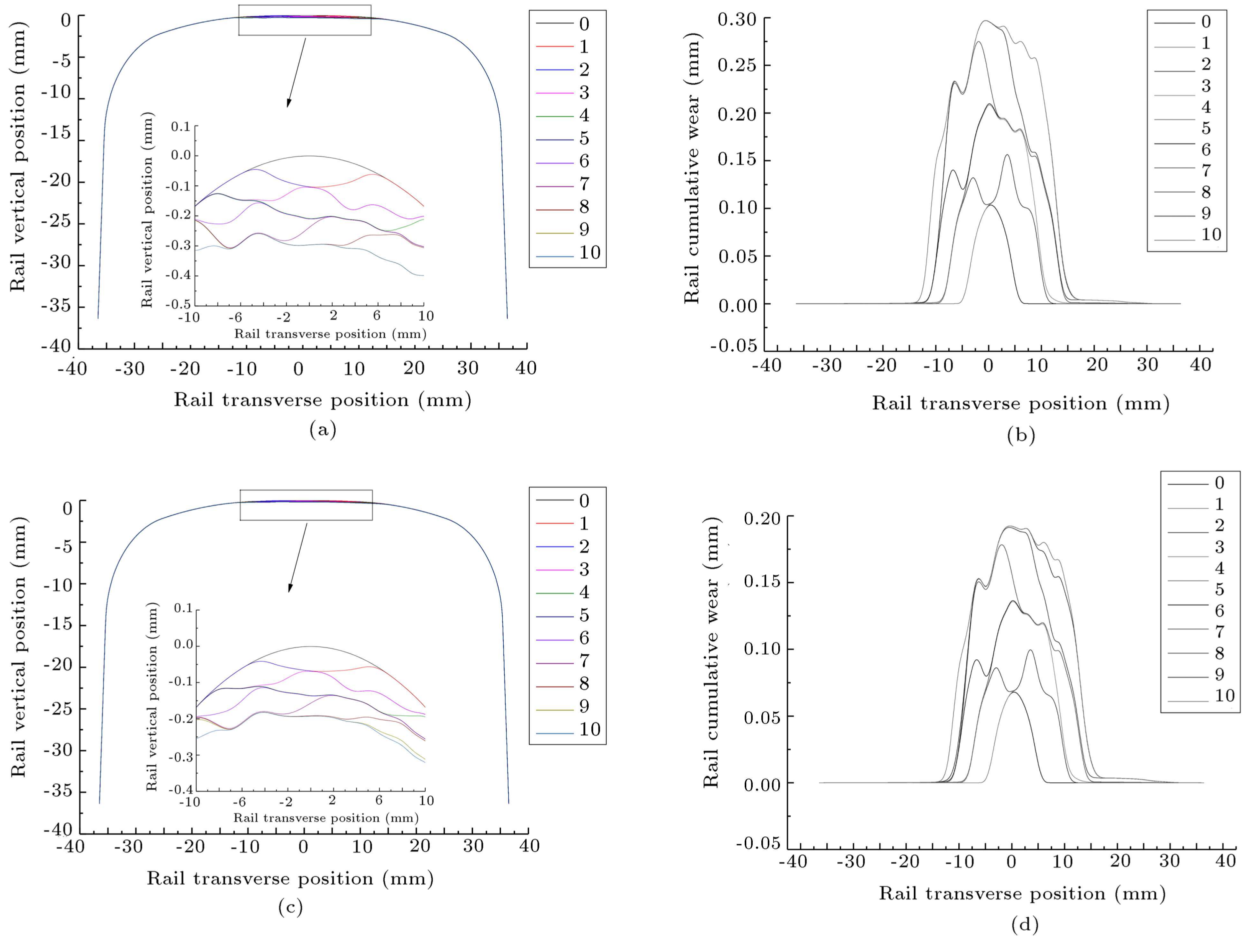

Figure 8. Right rail: (a) Rail profile diagram (trough), (b) rail cumulative wear diagram (trough), (c) rail profile diagram (crest), and (d) rail cumulative wear diagram (crest).

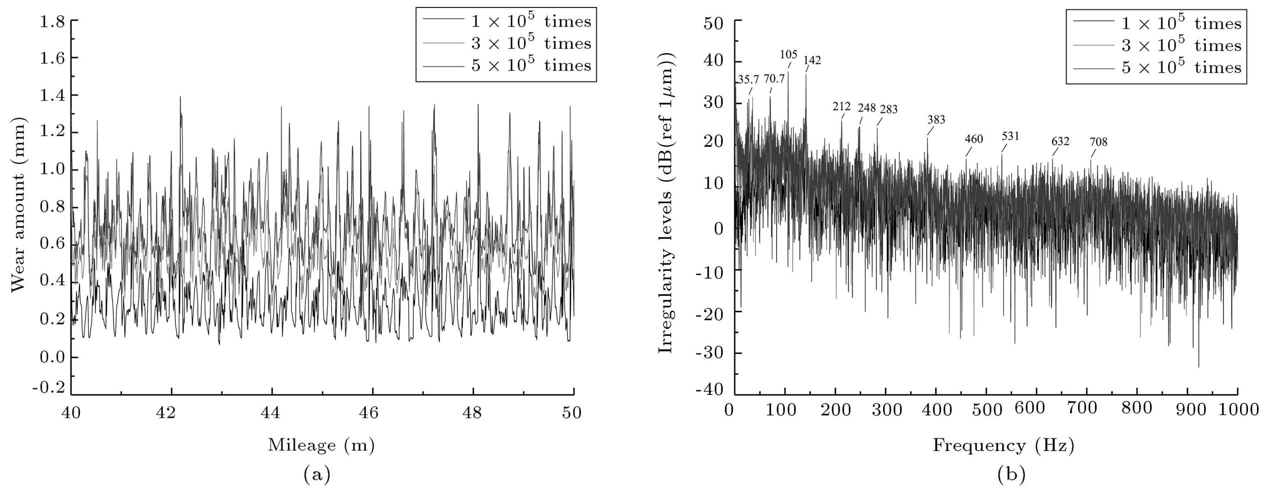

Figure 9. Time-frequency curves of corrugation characteristics: (a) Wear development curve and (b) irregularity levels.

of rail wear corresponding to other relevant frequencies. It can also be seen from Figure 9(b) and Figure 10(b) that the irregularity levels of 37.47 dB and 33.35 dB corresponding to the characteristic frequencies of 71.1 Hz and 35.7 Hz in Mode 2 are greater than those of 31.66 dB and 31.01 dB corresponding to 70.7 Hz and 35.7 Hz in Mode 1. However, compared with the irregularity levels of 37.67 dB and 36.89 dB corresponding to the main characteristic frequencies of 105 Hz and 142 Hz in Mode 1, the irregularity levels

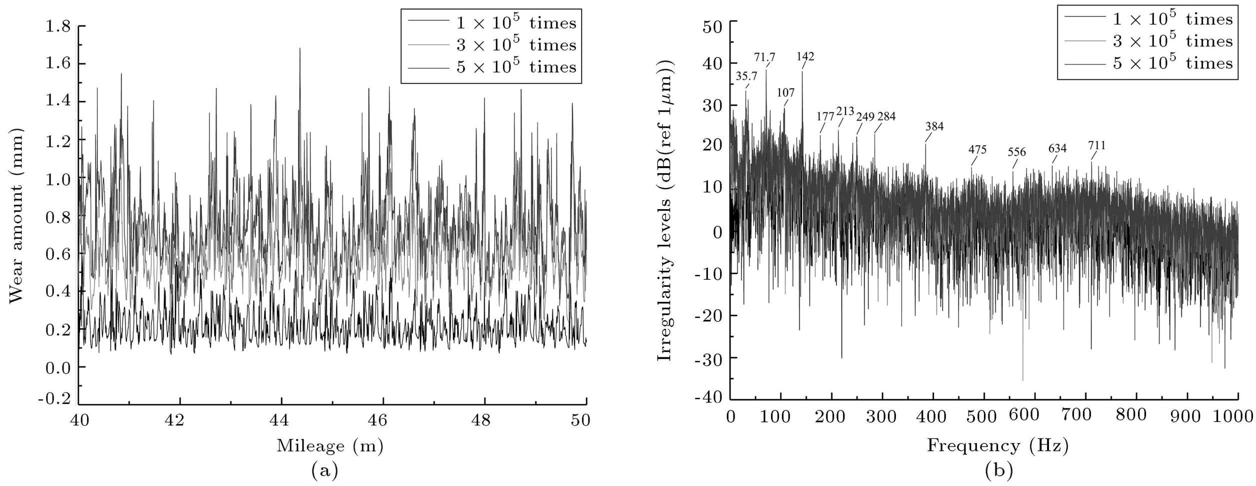

Figure 10. Time-frequency curves of corrugation characteristics: (a) Wear development curve and (b) irregularity levels.

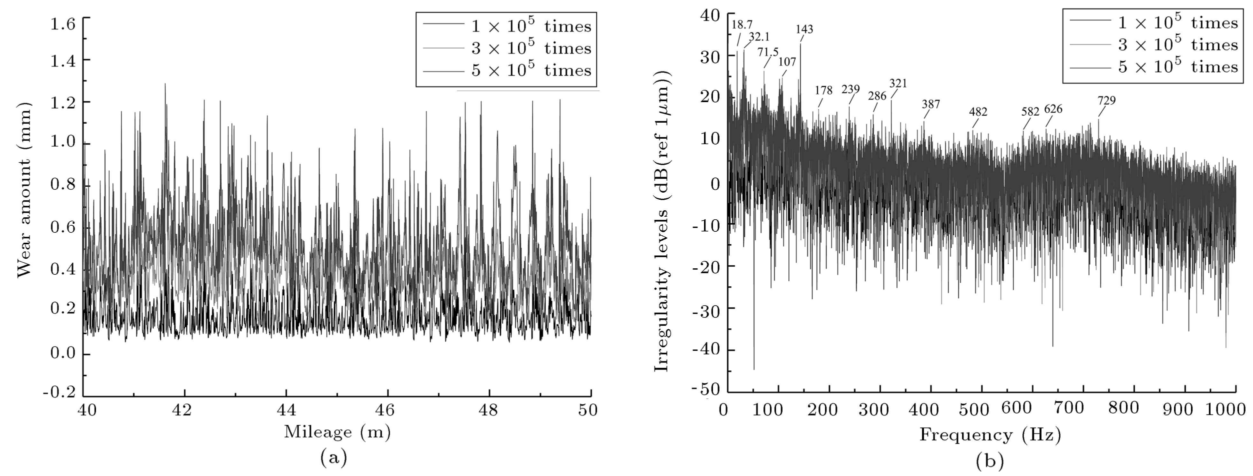

Figure 11. Time-frequency curves of corrugation characteristics: (a) Wear development curve and (b) irregularity levels.

of 37.47 dB and 36.77 dB corresponding to the main characteristic frequencies of 71.1 Hz and 142 Hz in Mode 2 are decreased, which is consistent with the conclusion that the rail wear of the discrete passing speed is smaller than that of the constant passing speed.

6. Conclusions

Based on the vehicle-track coupled model and the wear calculation model, the rail corrugation development characteristics of the tangential track with track-vibration-absorber fasteners at different passing speeds are analyzed using the development characteristics of rail profile wear and the longitudinal characteristics of rail wear development. The main conclusions are as follows:

1. When the iteration times increased, the wear ranges of the left and right rails were similar, mainly in the surface area of the railhead, and the wear depths of the left and right rails at the corrugation trough/crest position were close;
2. The rail profile wear depths and wave depth amplitudes at the corrugation trough/crest position of passing speed Modes 2 and 3 decreased significantly compared with those of Mode 1, which shows that the change of vehicle passing speed has a great impact on the rail profile wear of track-vibration-absorber fastener track. The discrete passing speed could significantly reduce the rail profile wear compared with the constant passing speed;
3. With the increase of vehicle running times, the characteristic frequencies of corrugation did not change under different passing speed modes. This characteristic reflects the fixed frequency feature of corrugation. The irregularity levels corresponding to characteristic frequencies of the longitudinal development of rail wear under three passing speed modes decreased in turn, which shows that the discrete passing speed modes can effectively

decrease the development degree of rail wear at the characteristic frequencies compared with the constant passing speed mode.

Acknowledgments

This research was supported by the National Natural Science Foundation of China (No. 11772230).

References

1. Kalousek, J. and Johnson, K.L. "An investigation of short pitch wheel and rail corrugations on the Vancouver mass transit system", *Proceedings of the Institution of Mechanical Engineers, Part F: Journal of Rail and Rapid Transit*, **206**(26), pp. 127–135 (1992).
2. Ahlbeck, D.R. and Daniels, L.E. "Investigation of rail corrugations on the Baltimore metro", *Wear*, **144**(1–2), pp. 197–210 (1991).
3. Tassilly, E. and Vincent, N. "Rail corrugations: analytical model and field tests", *Wear*, **144**(1–2), pp. 163–178 (1991).
4. Torstensson, P.T. and Nielsen, J.C.O. "Monitoring of rail corrugation growth due to irregular wear on a railway metro curve", *Wear*, **267**(1), pp. 556–561 (2009).
5. Xiao, H., Yang, S., Wang, H.Y., et al. "Initiation and development of rail corrugation based on track vibration in metro systems", *Proceedings of the Institution of Mechanical Engineers, Part F: Journal of Rail and Rapid Transit*, **232**(9), pp. 2228–2243 (2018).
6. Grassie, S.L. and Kalousek, J. "Rail corrugation: characteristics, causes and treatments", *Proceedings of the Institution of Mechanical Engineers, Part F: Journal of Rail and Rapid Transit*, **207**(1), pp. 57–68 (1993).
7. Grassie, S.L. "Rail corrugation: advances in measurement, understanding and treatment", *Wear*, **258**(7–8), pp. 1224–1234 (2005).
8. Grassie, S.L. "Rail corrugation: characteristics, causes, and treatments", *Proceedings of the Institution of Mechanical Engineers, Part F: Journal of Rail and Rapid Transit*, **223**(6), pp. 581–596 (2009).
9. Tanaka, H. and Miwa, M. "Modeling the development of rail corrugation to schedule a more economical rail grinding", *Proceedings of the Institution of Mechanical Engineers, Part F: Journal of Rail and Rapid Transit*, **234**(4), pp. 370–380 (2020).
10. Fourie, D., Frohling, R., and Heyns, S. "Railhead corrugation resulting from mode-coupling instability in the presence of veering modes", *Tribology International*, **152**, p. 106499 (2020).
11. Sadeghi, J., Rabiee, S., and Khajehdezfuly, A. "Effect of rail irregularities on ride comfort of train moving over ballast-less tracks", *International Journal of Structural Stability and Dynamics*, **19**(6), p. 1950060 (2019).
12. Jin, X.S., Wen, Z.F., Wang, K.Y., et al. "Effect of a scratch on curved rail on initiation and evolution of rail corrugation", *Tribology International*, **37**(5), pp. 385–394 (2004).
13. Jin, X.S., Wen, Z.F., and Wang, K.Y. "Effect of track irregularities on initiation and evolution of rail corrugation", *Journal of Sound and Vibration*, **285**(1–2), pp. 121–148 (2005).
14. Wen, Z.F. and Jin, X.S. "Effect of track lateral geometry defects on corrugations of curved rails", *Wear*, **259**(7), pp. 1324–1331 (2005).
15. Yan, Z.Q., Markine, V., Gu, A.J., et al. "Optimization of the dynamic properties of ladder track to minimize the chance of rail corrugation", *Proceedings of the Institution of Mechanical Engineers, Part F: Journal of Rail and Rapid Transit*, **228**(3), pp. 285–297 (2014).
16. Chen, G.X., Zhang, S., Wu, B.W., et al. "Field measurement and model prediction of rail corrugation", *Proceedings of the Institution of Mechanical Engineers, Part F: Journal of Rail and Rapid Transit*, **234**(4), pp. 381–392 (2020).
17. Chen, G.X. "Friction-induced vibration of a railway wheelset-track system and its effect on rail corrugation", *Lubricants*, **8**(2), p. 18 (2020).
18. Yao, H.M., Shen, G., and Cui, W. "Grinding method for rail corrugation in curved track", *Journal of Tongji University (Natural Science)*, **47**(8), pp. 1162–1167 (2019).
19. Hei, Y.J. "Analysis and treatment of fastener defects caused by metro rail corrugation", *Railway Engineering*, **59**(8), pp. 150–153 (2019).
20. Liu, X.G. and Wang, P. "Investigation of the generation mechanism of rail corrugation based on friction induced torsional vibration", *Wear*, **468–469**, 203593 (2021).
21. Song, X.L., Qian, Y., Wang, K.Y., et al. "Effect of rail pad stiffness on vehicle-track dynamic interaction excited by rail corrugation in metro", *Transportation Research Record*, **2674**(6), pp. 225–243 (2020).
22. Ma, C.Z., Gao, L., Xin, T., et al. "The dynamic resonance under multiple flexible wheelset-rail interactions and its influence on rail corrugation for high-speed railway", *Journal of Sound and Vibration*, **498**, 115968 (2021).
23. Wang, Y.R. and Wu, T.X. "Effect of vibration wave reflections between wheels and tracks with high-elastic fasteners on short pitch rail corrugation", *Journal of Vibration and Shock*, **39**(6), pp. 29–36 (2020).
24. Lei, Z.Y., Wang, Z.Q., Li, L., et al. "Rail corrugation characteristics of the common fastener track in metro", *Journal of Tongji University (Natural Science)*, **47**(9), pp. 1334–1340 (2019).
25. Lei, Z.Y. and Wang, Z.Q. "Generation mechanism and development characteristics of rail corrugation of cologne egg fastener track in metro", *KSCE Journal of Civil Engineering*, **24**(6), pp. 1763–1774 (2020).

26. Piotrowski, J. and Kik, W. "A simplified model of wheel/rail contact mechanics for non-Hertzian problems and its application in rail vehicle dynamic simulations", *Vehicle System Dynamics*, **46**(1–2), pp. 27–48 (2008).

27. Li, X. "Study on the mechanism of rail corrugation on subway track", Southwest Jiaotong University, Chengdu (2012).

28. Zhao, X.L., Wu, Y., Guo, T., et al. "Statistical law of wheel polygonal wear and analysis of key influencing factors", *Journal of Vibration, Measurement and Diagnosis*, **40**(1), pp. 48–53,202 (2020).

Biographies

Zhiqiang Wang was born in Zhangjiakou, Hebei, China in 1993. He received his BS from Chang'an University in 2017, his MS from Tongji University in 2020. He is currently a PhD candidate at Tongji University. His research interests include the wheel-rail relationship, rail vehicle dynamics, vibration, and noise and track structure.

Zhenyu Lei was born in Chengdu, Sichuan, China in 1970. She received her BS from the Chengdu University of Science and Technology in 1994, her MS and PhD from the Southwest Jiaotong University in 1998 and 2001. From 2002 to 2003, she was a Post-Doctor at the School of Transportation Engineering, Tongji University, China. Her interests include structural dynamics, track disease prevention, and vehicle system dynamics. She is currently at Tongji University. In 2017, she received a research project grant from the National Natural Science Foundation of China.